

Establishing Reality-Virtuality Interconnections in Urban Digital Twins for Superior Intelligent Road Inspection

Yikang Zhang^{ID}, Chuang-Wei Liu^{ID}, Jiahang Li^{ID}, Yingbing Chen^{ID},
Jie Cheng^{ID}, Rui Fan^{ID}, *Senior Member, IEEE*

Abstract—Road inspection is essential for ensuring road maintenance and traffic safety, as road defects gradually emerge and compromise road functionality. Traditional methods, which rely on manual evaluations, are labor-intensive, costly, and time-consuming. Although data-driven approaches are gaining traction, the scarcity and spatial sparsity of road defects in the real world pose significant challenges in acquiring high-quality datasets. Existing simulators designed to generate detailed synthetic driving scenes, however, lack models for road defects. Furthermore, advanced driving tasks involving interactions with road surfaces, such as planning and control in defective areas, remain underexplored. To address these limitations, we propose a system based on Urban Digital Twin (UDT) technology for intelligent road inspection. First, hierarchical road models are constructed from real-world driving data, creating highly detailed representations of road defect structures and surface elevations. Next, digital road twins are generated to create simulation environments for comprehensive analysis and evaluation. These scenarios are subsequently imported into a simulator to enable both data acquisition and physical simulation. Experimental results demonstrate that driving tasks, including perception and decision-making, can be significantly improved using the high-fidelity road defect scenes generated by our system.

Index Terms—intelligent road inspection, urban digital twins, data acquisition, physical simulation

I. INTRODUCTION

THE assessment of road surfaces is critical for vehicle dynamics and driving performance [1]. Road defects, such as cracks and potholes, induce vertical vehicle vibrations, negatively impacting driving comfort and accelerating wear on vehicle components. Timely detection, repair, and maintenance of these defects are essential to ensure road functionality and traffic safety. Current road inspection methods face several

challenges [2]. The traditional manual visual inspection process, conducted by certified inspectors, is labor-intensive, time-consuming, and hazardous. Moreover, it significantly disrupts normal traffic flow, making it impractical for large-scale road condition assessments [3]–[5]. Although crowdsourcing approaches have been proposed to collect large volumes of defect detection data [6], most of this data consists solely of images, lacking additional sensor modalities. Furthermore, the quality of the collected data is often compromised by individual subjectivity. Given these limitations, there is a growing need for intelligent road inspection systems that are portable, multi-modal, and reliable.

Recent technological advancements have made intelligent road inspection using Urban Digital Twins (UDT) feasible. A UDT system reconstructs the semantic and geospatial properties of urban entities, such as roads and buildings [7]. These digital replicas are indispensable for various applications, including real-time monitoring and simulation. Furthermore, the interconnection between the physical and virtual worlds enables the automatic generation of well-annotated road data, which can be used to train intelligent road inspection models.

Despite these advancements, existing virtual engines, such as CARLA [8] (based on Unreal Engine 4), typically represent roads as 2D planar surfaces. To effectively model road unevenness for perception and planning tasks, it is necessary to reconstruct the 3D structures of simulation assets using real-world data. Given the varying scale of road entities, this challenge can be divided into two parts: creating hierarchical road models using multi-modal data from different sensors, and generating digital road twins for simulation scenarios.

Once a UDT system is developed, a key question arises: can the synthetic data be used to evaluate downstream driving tasks, including perception and decision-making? For perception, models pre-trained on synthetic data demonstrate the ability to generalize to real-world data. Beyond replicating existing scenes, random combinations of road models create novel scenarios that enhance generalization. For planning, we propose a new research area focused on intelligent vehicle systems navigating defected road regions to improve both safety and comfort. Severe road defects can be treated as obstacles in avoidance tasks, requiring collision detection for the vehicle’s wheels rather than its entire body. In scenarios where traversal through defects is unavoidable, speed control can help mitigate vehicle vibrations.

This research was supported by the National Natural Science Foundation of China under Grants 62473288 and 62233013, the Fundamental Research Funds for the Central Universities, and Xiaomi Young Talents Program. (Corresponding author: Rui Fan)

Yikang Zhang, Chuang-Wei Liu, Jiahang Li and Rui Fan are with the College of Electronics & Information Engineering, Shanghai Research Institute for Intelligent Autonomous Systems, the State Key Laboratory of Intelligent Autonomous Systems, and Frontiers Science Center for Intelligent Autonomous Systems, Tongji University, Shanghai 201804, China. Yingbing Chen is with Individualized Interdisciplinary Program, Division of Emerging Interdisciplinary Areas, HKUST. Jie Cheng is with the Department of Electronic and Computer Engineering, HKUST, Hong Kong SAR (e-mails: {yikangzhang, cwliu, lijiahang617}@tongji.edu.cn, {ychengz, jchengai}@connect.ust.hk, rui.fan@ieee.org).

A. Contributions

To address the aforementioned challenges, we develop an UDT system that enables Reality-Virtuality Interconnection (RVI), specifically tailored for intelligent road inspection. This system not only reconstructs digital twins of road entities for data acquisition, but also generates simulation scenes of defected road models for evaluating perception and decision making methods. The contributions of this study span five key aspects: equipment, algorithm, simulator, dataset, and benchmark. As illustrated in Fig. 1, we develop a portable, multi-sensor experimental setup, equipped with a Livox Mid-360 LiDAR, two FLIR BFS-U3-31S4C cameras, and a DETA100D4G GNSS RTK module. This setup can be mounted on any vehicle, enabling multi-modal, high-quality road data collection in real-world scenarios. The collected data is processed using a LiDAR-Inertial Odometry (LIO) algorithm [9] to construct and continuously update a large-scale 3D map of the road scene. Additionally, a highly accurate stereo matching algorithm [10] is employed to generate dense 3D point clouds of road defects. To model the interconnection between reality and virtuality for urban entities, we develop two key modules: a hierarchical road model creator and a digital road twin generator. The former module extracts road defect structures and undamaged surface elevations from real-world sensor data, while the latter creates high-fidelity scenes for data collection and physical simulation. Specifically, we integrate varying-scaled road entities into a unified road surface model, ensuring no mesh collisions or face isolation for physical simulation. Mesh boundaries are carefully managed to segment 3D models into distinct simulation asset groups for semantic acquisition by the simulator. These assets replace simplified planar road models in the Unreal Engine 4 platform to simulate realistic road scenes. Given the sporadic occurrence of real-world road defects and the challenges inherent in collecting and labeling large-scale, multi-modal, high-quality road data with defects, our simulator can generate an unlimited amount of synthetic road data with realistic structure under diverse weather and lighting conditions. For perception tasks, we create a comprehensive dataset containing semantic and instance-level annotations, along with ground truth data for depth, event, and surface normals, to benchmark State-of-The-Art (SoTA) Deep Neural Networks (DNNs) for intelligent road inspection. Furthermore, unlike current autonomous driving tasks that primarily focus on obstacles impacting the vehicle’s body, our system evaluates decision-making strategies for “negative obstacles”, which consider only wheel-level collisions as constraints. Path planning algorithms are assessed for avoidance, and speed control strategies are analyzed for traversing road defects while maintaining driving comfort. Experimental results demonstrate that the optimal traversing speed varies depending on the specific characteristics of each defect.

In a nutshell, our main contributions are as follows:

- We design a UDT system for road inspection, including a portable multi-modal sensor equipment for real-world data collection, and a CARLA-based road defect simulator for data acquisition and physical simulation.

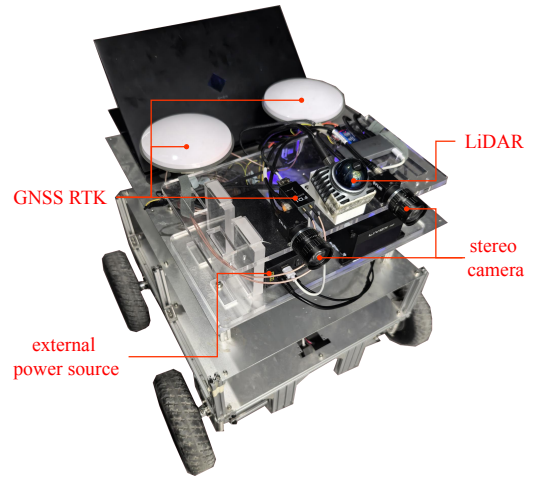


Fig. 1. The sensor setup includes a LiDAR, a stereo camera pair, and a GNSS RTK module, all powered by an external battery. A high-performance laptop is used for data processing.

- We propose a pipeline to autonomously construct hierarchical road models and generate digital road twins, enabling simulation for driving tasks such as perception, planning, and control in defected road conditions.
- We establish a new research paradigm for road scene reconstruction. In addition to generating diverse and well-annotated synthetic data, our system supports driving tasks that physically interact with road surfaces.

The remainder of this article is structured as follows: Sect. II reviews relevant research works. Sect. III and Sect. IV introduce the proposed sensor equipment and UDT system for intelligent road inspection, respectively. Sect. V presents the simulation setup and experimental results for driving tasks using the UDT system. Finally, Sect. VI concludes the study and discusses potential directions for future research.

II. RELATED WORKS

A. Intelligent Road Inspection

Traditional road inspection is typically carried out by structural engineers or certified inspectors, which is often subjective, inefficient, expensive, and sometimes hazardous [2]. To address these challenges, researchers have focused on developing intelligent road inspection systems that can recognize, localize, and reconstruct road defects efficiently, accurately, and objectively [11]. Data acquisition is the initial step in intelligent road inspection. Some methods mount sensors on the rear of the vehicle with a downward-facing view, targeting the road surface with a known distance, including single cameras [12], [13], stereo camera pairs [14], laser scanners [15] and laser pointers [16]. However, these specialized sensor configurations are restricted to dedicated inspection vehicles, limiting their scalability, timeliness, and widespread applicability. Alternatively, crowdsourcing approaches can gather extensive data from users’ daily driving. In such setups, sensors are forward-facing, enabling dual functionality for driving perception and road inspection. For instance, [17] employs LiDAR on the hood to detect road unevenness, while [18]

and [19] reconstruct forward 3D road surfaces using stereo cameras. Additionally, smartphone applications have emerged as a practical data source for road inspection [20].

Numerous computer vision-based algorithms have been developed for road defect detection. Classical 2D image processing methods have been widely explored, extracting damaged road areas from segmented foregrounds based on geometric and textural assumptions [19], [21]. For instance, to detect obstacles on non-flat road geometries, V-disparity [22] is employed. Subsequently, [10] and [3] refined these representations using disparity transformation algorithms to improve detection accuracy. However, such methods are sensitive to environmental factors that violate their underlying assumptions. 3D point cloud modeling and segmentation have also been employed to detect road irregularities. Camera-based approaches reconstruct dense 3D road point clouds and interpolate them into planar or quadratic surfaces [23]–[25]. LiDAR-based methods have been utilized for road roughness perception [17], [26], while road patches traversed by a vehicle’s tires are segmented to identify irregularities such as bumps and potholes [27]. With the rise of machine and deep learning, data-driven approaches have become the dominant techniques. Backbones such as Inception-v2 [28], MobileNet [29], ResNet [30], and RetinaNet [31] have been widely adopted for image classification and object detection for road defects. Image segmentation methods have also been proposed based on the networks, ranging from fully convolutional networks to graph attention-based models [4], [32], [33]. However, the performance of these data-driven methods heavily depends on the quality of the dataset. Due to the rarity and sparse distribution of road defects, capturing sufficient annotated data for training remains a significant challenge. Developing cost-effective methods to address this limitation is critical for advancing intelligent road inspection systems.

B. Urban Digital Twins

Digital Twin (DT), originally developed for cyber-physical integration in factories, connects real and virtual products through advanced data communication technologies [34], [35]. With the rapid advancement of digital transformation, the applications of DT technology have expanded across various domains, including smart manufacturing [36], advanced medical healthcare [37], and intelligent urban planning [38]. Leveraging advantages such as real-time monitoring [39], fast simulation, [40] and troubleshooting [41], DT technology applied to urban entities integrates data from multiple sensors and creates virtual models to address road anomalies [42]. These capabilities are exemplified by applications such as intelligent road inspection [43]. Extensive research has been conducted on urban entities using digital twin technology. For example, [44] proposed a pavement crack segmentation approach based on 3D edge detection within digital twins. [45] developed a cognitive twin of a pavement structure using data acquired from unmanned aerial vehicles for damage detection. Furthermore, [46] introduced a digital twin model capable of generating virtual distress data for asphalt pavements, while [47] presented a bridge management system leveraging digital

twins for precise bridge inspection. Recent studies have also achieved large-scale reconstruction of explicit road surface meshes, recovering both geometry and texture [48], [49]. However, most research treats digital twins of road defects and surfaces as individual reconstruction tasks. In contrast, our work integrates defective road entities at the scene level, creating comprehensive simulation environments specifically tailored for autonomous driving applications.

III. MULTI-MODAL DATA ACQUISITION

We employ a portable, multi-sensor, frame-aligned experimental setup (see Fig. 1) to capture various modalities of data. In the setup, the LiDAR generates sparse 3D point clouds, the IMU measures linear acceleration, angular velocity, as well as magnetic field strength, and the stereo camera produces dense disparity maps, where each disparity value is inversely proportional to depth. Rapid sensor movement can cause frame misalignment. Therefore, a GNSS RTK module is used for satellite time correction. A synchronized system clock signal, along with timestamp messages, is broadcast to all sensors to ensure accurate temporal alignment. The pose of the experimental setup is estimated using FAST-LIO [9], a state-of-the-art real-time LiDAR-inertial odometry algorithm. The following prediction model f and observation model h are utilized for state estimation:

$$\begin{cases} \mathbf{x}_k = f(\mathbf{x}_{k-1}, \mathbf{u}_k) + \mathbf{w}, \\ \mathbf{z}_k = h(\mathbf{x}_k) + \mathbf{v}, \end{cases} \quad (1)$$

where \mathbf{u}_k represents the IMU measurements at timestamp k , \mathbf{w} and \mathbf{v} respectively denote system and observation noises, the system state \mathbf{x}_k at timestamp k includes position, velocity, rotation, accelerometer bias, gyroscope bias, and the gravity vector, and the observation \mathbf{z}_k at timestamp k denotes the distance between LiDAR feature points and their corresponding local planes in the estimated map. The FAST-LIO algorithm uses a tightly-coupled iterated extended Kalman filter to update the gain matrix \mathbf{K} , resulting in the refined error state $\delta\mathbf{x}_k$ and predicted state $\hat{\mathbf{x}}_k$ as follows:

$$\begin{cases} \delta\mathbf{x}_k = \mathbf{K}(\mathbf{z}_k - \mathbf{h}(\hat{\mathbf{x}}_k)), \\ \mathbf{x}_k = \hat{\mathbf{x}}_k + \delta\mathbf{x}_k. \end{cases} \quad (2)$$

With pre-estimated extrinsic matrices, sensor frames are spatially and temporally aligned, enabling the acquisition of multi-modal data for our UDT system.

IV. URBAN DIGITAL TWIN SYSTEM

A. System Overview

Our proposed UDT system consists of two main components: a hierarchical road model creator (detailed in Sect. IV-B) and digital road twin generator (detailed in Sect. IV-C).

For the first component, the geometric and texture information of physical entities are extracted from frame-aligned stereo images and LiDAR point clouds, captured using the aforementioned equipment. The hierarchical road mesh creator utilizes this data to generate virtual road models, defined as $\mathcal{M} = \Phi(\mathcal{G}, \mathcal{S})$, where \mathcal{G} denotes the point clouds within a region of interest captured by the LiDAR and stereo camera, and

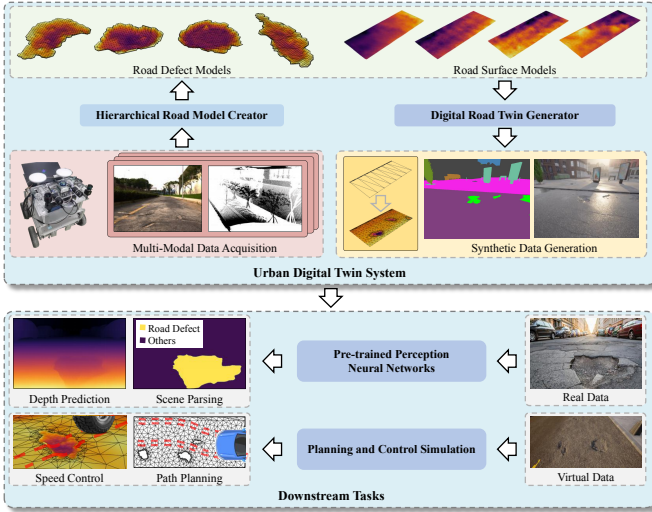


Fig. 2. The UDT system is composed of two components. The hierarchical road model creator autonomously reconstructs 3D defect models and non-defective road surfaces from the physical world, while the digital road twin generator produces virtual entities for a diverse, well-annotated environment.

\mathcal{S} represents the semantic masks produced using Grounded-SAM [50] and an unsupervised transformed disparity map segmentation algorithm [3]. In existing simulators, such as CARLA, roads are typically modeled as planar surfaces, resulting in meshes that lack sufficient granularity. To accurately represent the unevenness of physical roads, a collection of non-planar meshes must be reconstructed, as illustrated in Fig. 2. Each mesh consists of a set of triangular faces, with each face defined by three vertices v and three edges e . Generating meshes for an entire road using the stereo camera is computationally complex and memory-intensive, while using LiDAR for this task is impractical for road defects due to the limited granularity of sparse point clouds. When road defects are absent, coarse-grained meshes are preferred, with each vertex corresponding to a 3D point from the sparse point cloud generated by the LiDAR. In contrast, when road defects are present, fine-grained meshes are required, where each vertex corresponds to a 3D point from the dense point cloud generated by the stereo camera. Therefore, we design a hierarchical road model creator with two processing streams, one for road defects and the other for non-defective surfaces.

Subsequently, the digital road twin generator converts the models into simulation assets for scene generation. In the simulator, RGB images are rendered from objects through a pipeline that processes pixel data in stages, such as occlusion culling, vertex shading, and rasterization. To ensure geometric consistency, adjacent meshes must align seamlessly in the scene, with no gaps or overlaps. However, the meshes cannot be modeled as a whole, as semantic annotations require each simulation instance to be labeled with a class ID corresponding to its asset. To provide this reference, the outputs of the hierarchical road model generator are disassembled and saved as individual entities. Finally, a diverse virtual environment is generated using the road entities. Existing simulation scenes, although based on over-simplified planar road surfaces, incor-

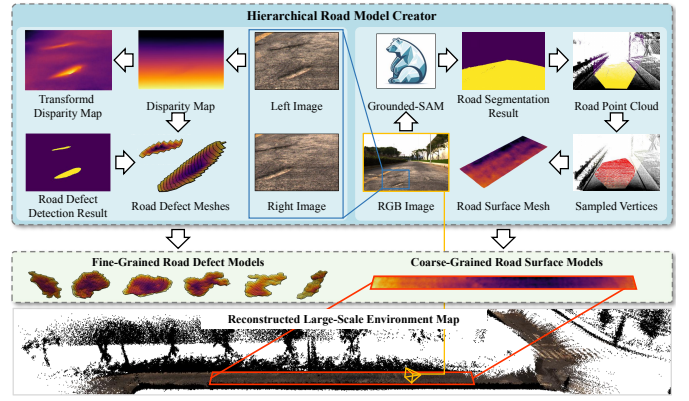


Fig. 3. Our hierarchical road model creator consists of two reconstruction streams. In the coarse-grained stream, semantic annotations are generated by Grounded-SAM, which filters LiDAR points for road surface mesh generation. The fine-grained stream reconstructs road defect models using transformed disparity maps derived from stereo images. The reconstructed results are stored in a library for future use.

porate built-in navigation features such as traffic lights and reference trajectories. To fully leverage these capabilities, our developed digital road twin generator integrates the detailed defect models with the planar road models and restores the elevation variations of physical roads.

With these two components, our UDT system produces well-annotated road scene data and enhances the comprehensive understanding of road scenes.

B. Hierarchical Road Model Creator

The hierarchical road model creator consists of two reconstruction streams, one for road defects and the other for non-defective surfaces, as illustrated in Fig. 3. The coarse-grained stream, focused on the reconstruction of non-defective road surfaces, follows a straightforward process. Semantic masks are generated from camera images using Grounded-SAM, with prompts such as “road” or “pavement”. LiDAR points are segmented based on these masks and fused across multiple frames. To achieve coordinate alignment, a horizontal ground plane is fitted to points from multiple road segments, assuming local elevation variations while maintaining overall flatness. A 3D downsampling operation is then applied to refine the vertices before meshing, accounting for density variations in the point clouds caused by redundant or missing observation views. Given the simple geometry of non-defective road surfaces, elevation can be decoupled from the planar coordinates. The mesh model is reconstructed by directly triangulating the 2D projection of vertices onto the horizontal plane. Vertex elevations are subsequently restored from the original point cloud, ensuring that the reconstructed surface accurately reflects real-world topography.

The stream for fine-grained road defects, unlike the non-defective road surfaces, requires dense geometric details. Although many neural networks are proposed for road defect detection from monocular images, semantic cues at the boundaries between defective and non-defective surfaces are often ambiguous, leading to artifacts such as isolated pixels

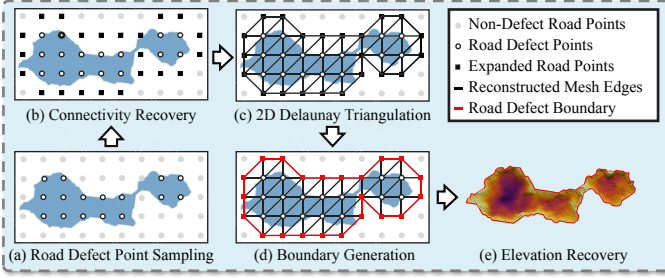


Fig. 4. Example of the road defect reconstruction process. Points are iteratively sampled until the entire road defect structure is covered, ensuring topological connectivity. Following triangulation, the boundary vertices are stored in a list with pseudo-heights, which are subsequently utilized by the digital road twin generator for model alignment.

or incomplete segmentation. Therefore, defect regions are extracted based on geometric cues, performed by transformed disparity maps derived from stereo images, which highlight spatial deviations from the planar patches of the road surface. Road defect instances are identified as connected components within the parsed scene. Instances with regular shapes, as shown in Fig. 3, can be reconstructed directly through grid-based sampling, similar to the first stream. However, defects with irregular shapes, as illustrated in Fig. 4, may introduce structural discontinuities, even when pixel connectivity is preserved. To address this issue, the sampled point set is expanded iteratively until the entire defect region is covered. Expanded points, belonging to the defect but lying on the non-defective region, are shared between adjacent meshes. If reconstructed separately, these duplicate boundary points could cause elevation mismatches, resulting in gaps or overlaps. Therefore, the boundary of the defect mesh is extracted and assigned a pseudo-height, which becomes active only when assembled with neighboring road surface meshes. A boundary edge is defined as an edge connected to only one face in the mesh, indicating that it forms the outer boundary or “hole” of the surface. All faces in the road defect model are traversed to identify such edges. Since boundary points are guaranteed to lie on the non-defective road surface, they can be used to fit a transformation matrix that aligns the defect model with the ground plane, ensuring that the pseudo-height is set to zero.

The outputs from the two reconstruction streams are compiled into a road model library. This design, with varying levels of granularity, ensures that the road meshes remain memory-efficient while retaining sufficient details.

C. Digital Road Twin Generator

Although road scenes can be accurately replicated, road defects are relatively rare in the physical world. To generate more diverse digital road twins, over-simplified road models from the simulator must be integrated with reconstructed road defect models, as illustrated in Fig. 5. First, the original road segment assets from the simulator, consisting primarily of planar meshes with simple polygonal shapes, are exported. The generated road defect models are then sampled with random poses and scales for integration. When merging the mesh mod-

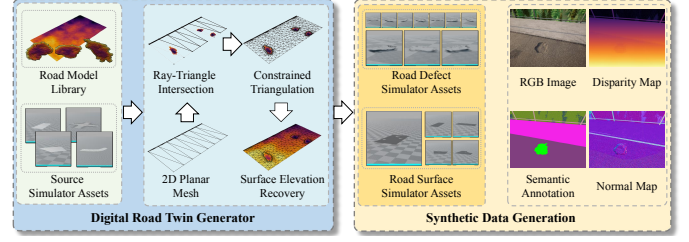


Fig. 5. The Digital Road Twin Generator integrates simulator assets with reconstructed road models. Road defect models are projected onto the 2D road mesh to eliminate intersecting faces. The 2D structure is reorganized using constrained Delaunay triangulation, preserving model boundaries. For compatibility with the simulator, the generator’s output is disassembled into individual road surface and defect asset groups, providing semantic references for the rendering pipeline.

els, intersecting triangular faces must be removed. However, because road segments are not always convex, simply removing all faces and remeshing could compromise their structural integrity. Therefore, defect models are projected vertically onto the road surface to accurately identify and remove only the intersecting triangles. The Möller-Trumbore algorithm [51] is typically used to detect ray-triangle intersections,

$$\mathbf{r}(t) = \mathbf{o} + t\mathbf{d} = (1 - u - v)\mathbf{p}_0 + u\mathbf{p}_1 + v\mathbf{p}_2, \quad (3)$$

$$s.t. \begin{cases} 0 \leq u \leq 1 \\ 0 \leq v \leq 1 \\ 0 \leq 1 - u - v \leq 1 \end{cases} \quad (4)$$

where ray \mathbf{r} originates from \mathbf{o} in direction \mathbf{d} with length t , and the triangle is determined by points $\mathbf{p}_0, \mathbf{p}_1, \mathbf{p}_2$. Rewriting (3) leads to:

$$\mathbf{o} - \mathbf{p}_0 = (\mathbf{p}_1 - \mathbf{p}_0)u + (\mathbf{p}_2 - \mathbf{p}_0)v - t\mathbf{d}, \quad (5)$$

which can be solved using Cramer’s Rule, where

$$t = \frac{(\mathbf{o} - \mathbf{p}_0) \times (\mathbf{p}_1 - \mathbf{p}_0) \cdot (\mathbf{p}_2 - \mathbf{p}_0)}{(\mathbf{o} - \mathbf{p}_0) \times (\mathbf{p}_2 - \mathbf{p}_0) \cdot (\mathbf{p}_1 - \mathbf{p}_0)}, \quad (6)$$

with similar solutions for u and v . With all intersecting faces removed, the defect models are positioned within the holes of the planar road mesh. The structure of the defect models remains fixed, except at the boundaries, which are assigned pseudo-height values. The remaining planar road surfaces must then be re-organized, typically through triangulation, which iteratively divides edges, samples vertices, and generates faces. However, as previously mentioned, mismatches may occur at the boundaries if adjacent meshes are reconstructed separately. To address this issue, the previously extracted boundaries are used as edge constraints to reconstruct the 2D structure of the road surface mesh using the constrained Delaunay triangulation algorithm [52]. Since the pseudo-height is set to zero, the defect model can be seamlessly aligned with the planar road surface, ensuring geometric consistency. For better realism and diversity, road surface elevations are restored from our model library. The height of each vertex is efficiently queried through a KD-Tree built from the reconstructed surface model. The final integrated 3D mesh is then split into individual assets, as required by the simulator, to provide semantic references.

Leveraging the hierarchical road model creator and the digital road twin generator described above, our UDT system bridges reality-virtuality interconnections to generate diverse, well-annotated simulation scenes featuring road defects. The virtual environment not only provides synthetic data to enhance perception networks that depend on comprehensive road surface data, but also enables physical simulation for decision-making tasks that interact directly with road surfaces. In the following section, we demonstrate these advancements by presenting perception tasks trained on synthetic data and decision-making tasks performed within our virtual environment.

V. EXPERIMENTAL RESULTS

A. Simulation Scene Setup

Based on sensor data collected from defected roads, our hierarchical road model creator generates a road model library containing 53 distinct road defect models with varying shapes and sizes. These models are integrated into city scenes within the simulator, replacing the original planar road surfaces. Specifically, 646 road segments are extracted from Town01. Subsequently, 1,000 defect instances are sampled and integrated into the scene using our digital road twin generator, with randomized scales, locations, and orientations. To accelerate the generation process, we leverage parallel processing. Using 24 13th Gen Intel(R) Core(TM) i7-13700K processors and 128 GB of RAM, the integration of road meshes for Town01 is completed in approximately 2 minutes. Finally, in Unreal Engine-based simulators, semantic references are accessed via asset paths. Therefore, the generated meshes are disassembled into individual entities: the 646 road meshes replace those in the original “road” group in Carla, while the 1,000 road defects are imported into a newly created “defect” group.

B. Perception Tasks

We design experiments for various perception tasks to demonstrate how synthetic data alleviates the scarcity of real-world road defect data and enhances of existing models.

1) *Semantic Segmentation*: We first evaluate single-modal semantic segmentation networks using real-world RGB images. The UDTIRI dataset [7], a real-world road defect dataset containing 1,000 semantically annotated images, is used for evaluation. Each image is captured from a unique perspective using various cameras. To replicate this diversity in the simulator, virtual sensor poses are randomly generated for each capture. Experiments are conducted on a single NVIDIA RTX 4090 GPU, evaluating six single-modal networks for image segmentation and road defect detection. All networks are pre-trained for 40,000 epochs using different ratios of synthetic data, followed by fine-tuning on 600 images from the UDTIRI dataset. Input images are cropped to 512×512 pixels. Although the dataset provides multiple object classes, only “background” and “pothole” are considered for this task. Network configurations follow the default settings of the MM-Segmentation benchmark [53]. For example, Mask2Former [54] is trained using the AdamW optimizer [55] with a polynomial learning rate decay strategy [56]. The learning rate starts at 10^{-4} with a weight decay of 5×10^{-2} . Mean

intersection over union (mIoU) is used as the evaluation metric to assess network performance.

TABLE I
mIoU(%) \uparrow OF SINGLE-MODAL SEMANTIC SEGMENTATION RESULTS WITH DIFFERENT RATIO OF SYNTHETIC DATA

Method	Synthetic/Real data ratio		
	0%	50%	100 %
Mask2Former [54]	77.08	79.79	80.07
PSPNet [57]	71.42	71.44	74.29
SegFormer [58]	75.16	75.96	76.94
SegNext [59]	79.68	79.84	80.63
Twins [60]	78.40	79.10	79.06
UperNet [61]	70.97	72.54	73.89

TABLE II
mIoU(%) \uparrow OF SEMANTIC SEGMENTATION RESULTS WITH DIFFERENT MODALITIES.

Method	RGB only	RGB+Depth	RGB+Normal	RGB+Event
RTFNet [62]	67.5	74.6	69.2	63.6
FuseNet [63]	66.6	78.7	53.9	58.5
MFNet [64]	72.0	80.1	90.6	72.3
SNE-RoadSeg [65]	67.4	78.8	94.5	73.5
RoadFormer [66]	90.3	94.8	96.1	90.6

Qualitative and quantitative results are presented in Fig. 6 and Table I, respectively. It is evident that pre-training with synthetic data significantly enhances segmentation accuracy, providing more precise boundaries and reducing the occurrence of false-positive regions. The results show that synthetic data generated by our UDT system positively impacts image-based road defect detection, increasing mIoU by up to 3%. Although the performance of Twins pre-trained with the full set of synthetic data slightly decreases 0.04 compared to the 50% subset, it still outperforms the non-pretrained model by 0.66%. This improvement alleviates the challenge posed by the limited availability of annotated real-world road defect data for road inspection models.

Single-modal prediction results from RGB images are often affected by environmental factors, such as lighting conditions. In contrast, multi-modal fusion is widely recognized as a method to enhance perception robustness, though capturing these modalities in the real world remains challenging. By leveraging the G-buffer in the rendering pipeline, we evaluate auxiliary modalities for road inspection, focusing on image segmentation for drivable areas, road defects, and backgrounds. An autopiloted vehicle is deployed in a simulated road defect scene with randomized surrounding vehicles and pedestrians. Sensors are mounted on the ego vehicle and oriented at a pitch angle of 30 degrees toward nearby road surfaces, capturing normal, depth, and event images. During data recording, dynamic weather conditions are simulated, continuously changing to enhance data variability. Since no real-world dataset provides such comprehensive information, the models are evaluated using synthetic data.

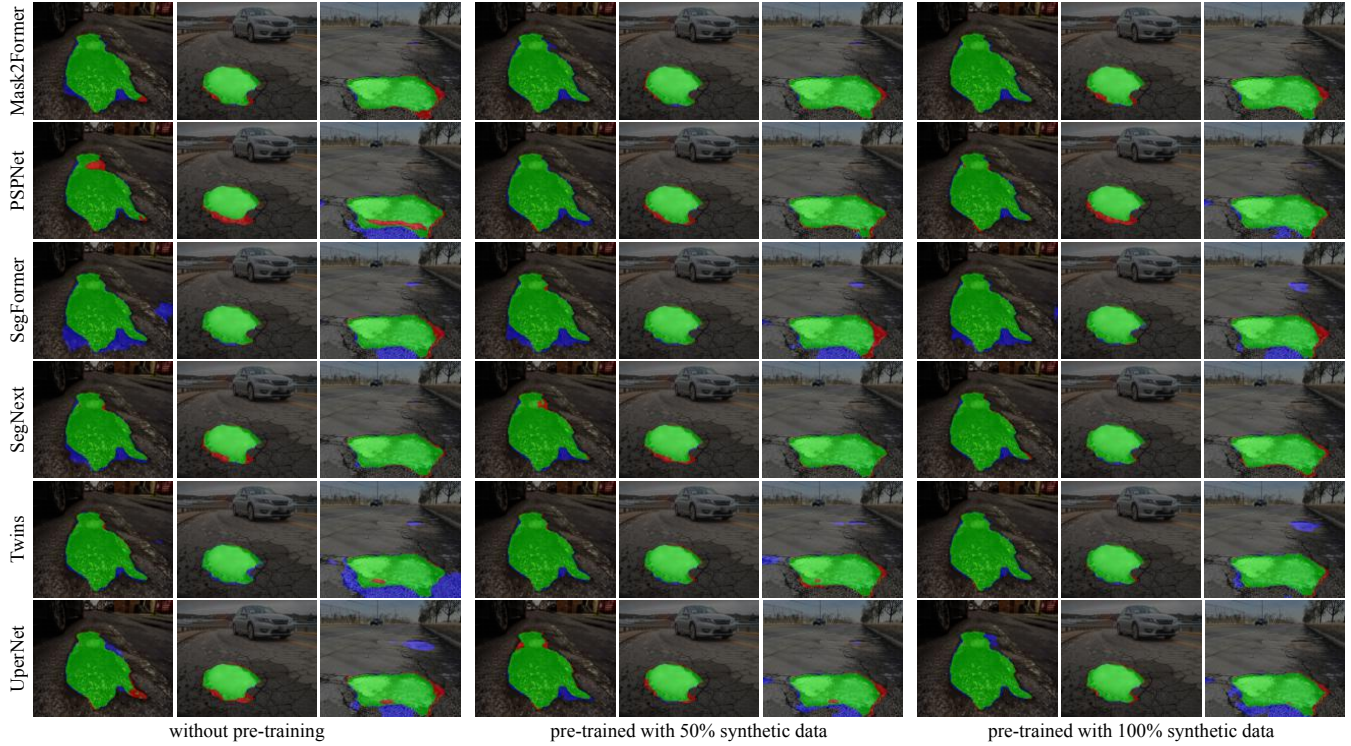


Fig. 6. Qualitative experimental results of semantic segmentation based on RGB images. The green areas in the image represent true-positive predictions, the blue areas represent false-positive predictions, and the red areas represent false-negative predictions.

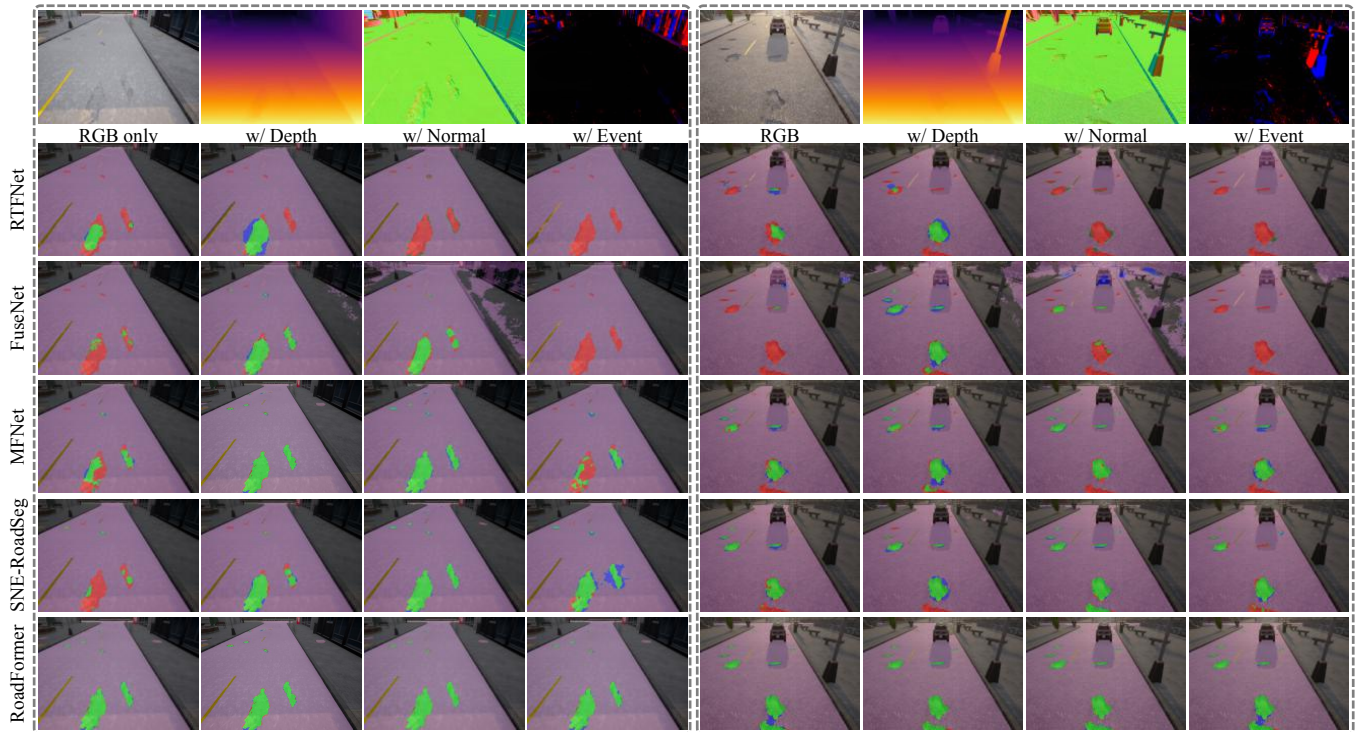


Fig. 7. Qualitative comparison between SoTA multi-modal networks on the synthetic data. The predicted drivable area is represented in purple. True-positive, false-positive, and false-negative classifications of road defects are shown in green, blue, and red, respectively.

TABLE III
COMPARISONS OF SoTA STEREO MATCHING NETWORKS WITH AND WITHOUT OUR PROPOSED SYNTHETIC DATA. THE BEST RESULTS ARE SHOWN IN BOLD TYPE.

Method	PEP(%) ↓		EPE(pixel) ↓	SSIM ↑	MSE ↓	PSNR(dB) ↑
	$\delta = 0.5$	$\delta = 1$				
PSMNet [67]	53.50	22.00	2.57	0.82	152.2	28.3
PSMNet+synthetic	7.61	3.59	0.67	0.90	93.5	30.9
AANet [68]	37.60	23.7	4.79	0.85	118.2	29.7
AANet+synthetic	9.36	5.30	0.61	0.91	93.4	30.8
LacGwc [69]	15.00	8.17	1.35	0.89	113.4	30.4
LacGwc+synthetic	6.11	2.92	0.55	0.90	96.0	30.7
IGEV [70]	8.14	4.99	0.83	0.90	102.9	30.8
IGEV+synthetic	3.17	1.59	0.23	0.91	92.5	30.9
ViTAStereo [71]	7.61	5.08	1.31	0.90	124.4	29.6
ViTAStereo+synthetic	3.14	1.61	0.22	0.91	91.6	30.9

As shown in Table II and Fig. 7, each additional modality is fused with RGB images in an RGB+X format. RGB+Depth provides the most generalized results, outperforming those trained using only RGB images by 4.5% to 12.1%. It also generates the most accurate true-positive predictions, demonstrating robust performance across all cases. This result is intuitive, as depth images directly capture the surface structure. Normal maps, which are highly sensitive to object surfaces, improve performance by 1.7% to 27.1% across most networks, except for FuseNet. Although useful in many cases, this sensitivity also introduces noise, leading to convergence issues. Fig. 7 shows that with the normal modality, FuseNet predicts the sidewalk as a noisy drivable area, resulting in poor mIoU performance. Simple fusion of event images across network channels is unstable. Although event images improve SNE-RoadSeg by 6.1%, they degrade FuseNet’s performance by 8.1%. This instability is likely due to event data being influenced by the vehicle’s driving speed, whereas RGB images assume static objects during exposure. To effectively utilize this modality, additional speed priors are required.

2) *Stereo Matching*: For stereo matching evaluation, we compare five SoTA networks to demonstrate the improvements enabled by our system. Similar to the single-modal segmentation experiments, these networks are pre-trained on synthetic data and fine-tuned using real-world data. Unlike individual road surface images, which can still be obtained through crowdsourcing applications, stereo images of road surface defects are exceedingly rare. To address this limitation, we fine-tune the networks using the KITTI dataset [72], a widely used driving dataset that lacks road defects.

Several metrics are selected for evaluation, including percentage of error pixels (PEP), which represents the percentage of incorrect disparities with respect to a tolerance of δ pixels, and end-point error (EPE), which measures the average disparity estimation error. Considering the domain gap, networks fine-tuned on KITTI may struggle with road defects. To further assess accuracy, mean squared error (MSE), structural similarity index (SSIM), and peak signal-to-noise ratio (PSNR) are compared between the predicted and ground truth disparity maps. The loss function, learning rate, and

optimizer settings are consistent with those reported in the corresponding publications [67]–[71].

Tables III presents the quantitative results tested on synthetic data. Nearly all networks pre-trained with our synthetic data demonstrate performance improvements. EPE is improved across all networks, with reductions ranging from 0.60 to 3.18. Although the improvement in PSNR is relatively modest, ranging from 0.1 to 2.6, qualitative results in Fig. 8 clearly show the noise difference. Networks trained solely on KITTI data perform poorly, often failing in challenging cases, such as the black areas predicted in the third image by PSMNet and AANet. In contrast, pre-trained networks produce smoother and more accurate predictions. These results confirm that our UDT system significantly enhances model performance for stereo matching tasks.

C. Decision Making Tasks

Two types of experiments are conducted: one for 2D path planning, where road defects are avoidable, and the other for speed control, where the vehicle must traverse defects.

1) *Path Planning*: In scenarios with ample road space and minimal opposing traffic, avoiding defects by following an alternative path is generally the preferred strategy. Unlike traditional obstacle constraints, road defects primarily impact the wheels rather than the vehicle body, allowing the vehicle to either bypass or glide over the defects. Consequently, collision detection at each time step is replaced by wheel-based checks. As shown in Fig. 9 (a), multiple defects are distributed along the road. The drivable area and defected regions are modeled as grid maps with a resolution of 0.2 m, and the vehicle model assumes a width of 2.0 m and a rear-to-front wheel distance of 3.0 m. Four widely used planning algorithms are compared: A* [73], RRT* [74], Lattice [75], and Hybrid A* [76]. The RRT* algorithm uses an expansion distance of 1.0 m. For the Lattice algorithm, lateral and longitudinal step sizes are set to 1.0 m and 5.1 m, respectively, with each node connecting to three adjacent nodes via a cubic spline curve. In Hybrid A*, a yaw grid resolution of 15 degrees is applied, and penalties for steering and lane changes are incorporated into the heuristic cost. Evaluation metrics are adapted from

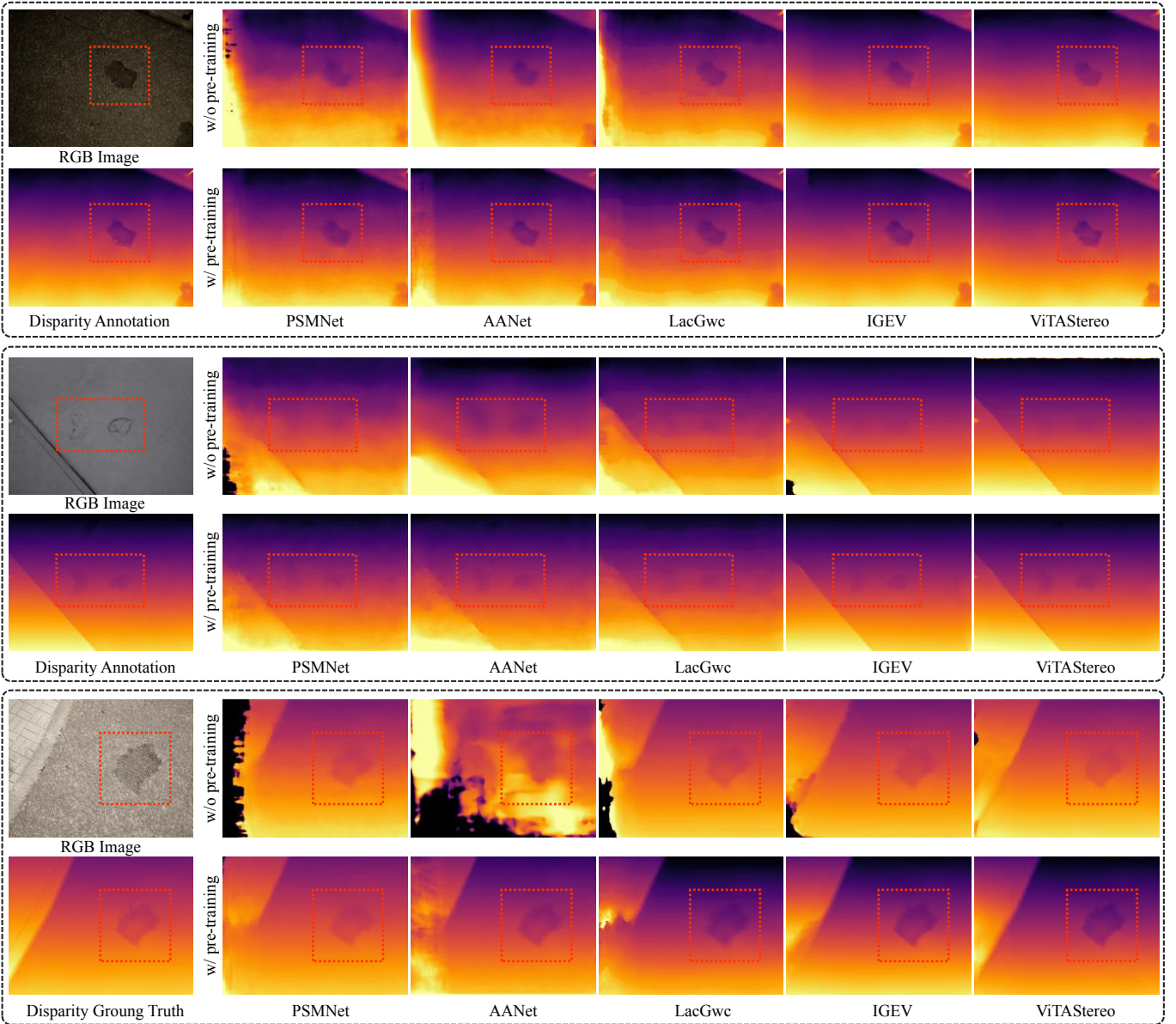


Fig. 8. Qualitative stereo matching results with and without pre-training using synthetic road defect data from the UDT system.

classical obstacle avoidance tasks. Path deviation quantifies the length difference between the planned path and the shortest possible path, typically the road’s midline. Path smoothness is calculated by averaging the angle changes along the trajectory, while obstacle clearance measures the mean distance between the vehicle’s wheels and the nearest road defects.

Quantitative and qualitative results of the generated paths are presented in Table IV and Fig. 9 (a). Notably, A* and RRT* do not account for vehicle kinodynamic constraints, resulting in relatively poor path smoothness, with values of 0.294 and 0.402, respectively. However, their discrete path points remain topologically reasonable. The paths generated by Hybrid A* and Lattice glide over defects p_0 and p_1 , which is justified in the given context. As one of the most commonly used planning algorithms in road scenarios, Lattice generates the shortest and

smoothest path, with a path deviation of 0.87 and a smoothness value of 0.047. However, because its grids and curves are pre-sampled, obstacles may not always be perfectly avoided. In contrast, Hybrid A* expands nodes iteratively at each step, achieving an obstacle clearance of 3.74, which ensures better safety distances. The trade-off, however, is that heuristic terms must be manually designed to suit specific scenarios.

2) *Speed Control*: In scenarios where changing lanes is risky, the vehicle must traverse road defects directly. In such cases, longitudinal speed becomes the only controllable variable to minimize vibrations. We customize these scenarios using our UDT system, where surface models of real-world roads are cropped into 40-meter sections, and integrated with randomly distributed road defects. With the aid of the simulator, road defects along the wheel trajectories can be pre-

TABLE IV
COMPARISON OF PATH PLANNING ALGORITHMS FOR ROAD DEFECT AVOIDANCE

Planner	path dev.(%)	path smoothness(rad/m)	obstacle clearance(m)
A*	7.46	0.294	3.69
RRT*	21.2	0.402	3.72
Lattice	0.87	0.047	2.62
Hybrid A*	1.05	0.054	3.74

cisely located, enabling informed speed control strategies. To measure vehicle vibrations caused by defected road surfaces, the collision settings for road entities in the simulator are configured to "use complex as simple," allowing collisions to be calculated for each triangular face between the road and tires during physical simulation. As shown in Fig. 9 (b), six-axis IMU data is recorded as the vehicle traverses defected road sections at a constant speed. During the process of a wheel falling into and exiting a road defect, it can be observed that the most affected parameters are vertical acceleration a_z , rotational velocity in roll ω_x and pitch ω_y . Subsequently, the vibration degree is defined as $g = \sqrt{\omega_x'^2 + \omega_y'^2 + \alpha a_z'^2}$, where α is set to 0.1 in this scenario. Quantitative results for traversing three road defects at different speeds are presented in Fig. 9 (c). The results indicate that, for large and severe defects such as p_2 , slowing down is the most effective strategy for driving comfort. Interestingly, for small and shallow defects, such as p_1 , increasing speed can also reduce vibrations. Although initially counterintuitive, this observation aligns with practical experience upon closer analysis.

VI. CONCLUSION AND FUTURE WORK

In this paper, we introduce a UDT system that leverages reality-virtual interconnections of road entities to advance intelligent road inspection. The system begins with the design of sensor equipment to capture data from defected road surfaces. A hierarchical road model creator is then used to generate detailed models of road defects and surfaces. These models are subsequently integrated into simulation scenes by a digital road twin generator, replacing the simplified planar roads commonly used in existing simulators. The proposed system provides unlimited, multi-modal, and well-annotated data for training road inspection networks, as well as a physical simulation environment for testing autonomous driving tasks under defected road conditions. Experimental results demonstrate that pre-training baseline perception networks with our synthetic data significantly improves their performance, addressing the scarcity of annotated real-world road defect data and supporting the development of robust inspection models. Additionally, decision-making strategies for navigating defected roads are evaluated. Common 2D path planning algorithms are analyzed for bypassing or gliding over road defects. When defects are unavoidable, vibration measurements under different traversal speeds reveal that optimal speed strategies vary based on the severity of the defect.

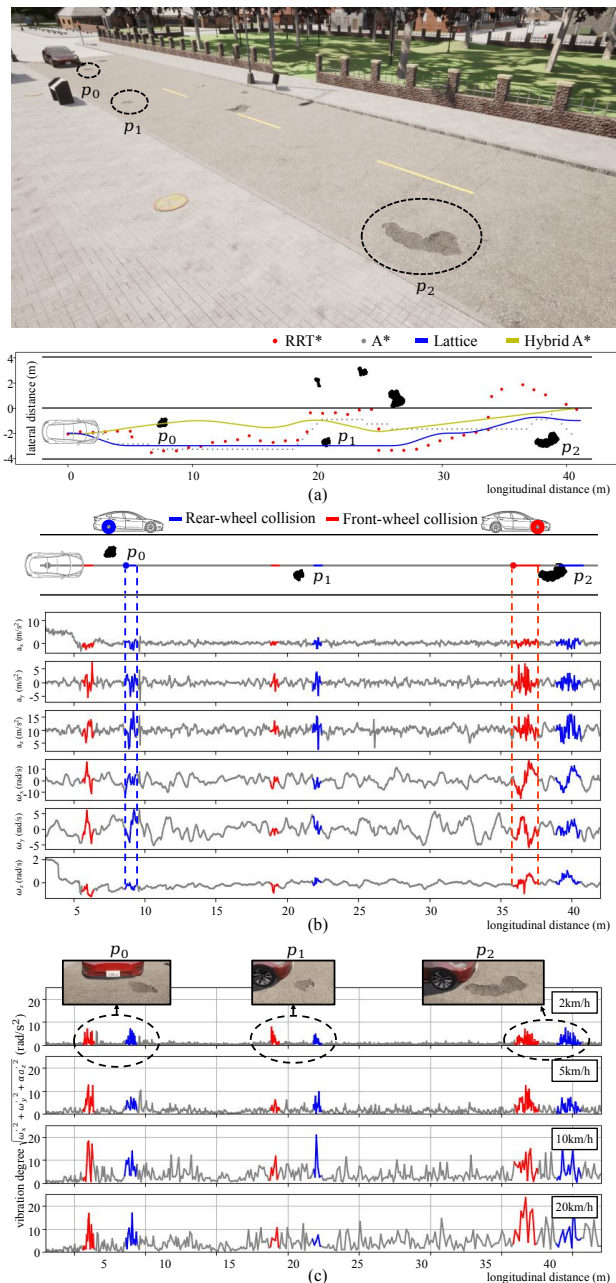


Fig. 9. Experiments on planning and control tasks using our UDT system. (a) Path planning for road defect avoidance, focusing on tire-ground collision constraints instead of vehicle body. (b) nertial measurements recorded while traversing road defects at a constant speed of 5 km/h. (c) Vibration degree evaluated over road defects with different traversing speeds.

Despite these advancements, several challenges remain. The sim-to-real gap is inevitable due to information loss during the rendering process, leading to synthetic data with artificial appearances. As a result, synthetic data is primarily limited to pre-training and must be supplemented with real-world data for fine-tuning. Future work could explore the use of explicit representations, such as 3D Gaussian Splatting (3DGS) [77], to replace the current rendering process with photorealistic novel view synthesis, while preserving the explicit geometric accuracy required for physical simulation.

REFERENCES

- [1] H. Guo, Z. Yin, D. Cao, H. Chen, and C. Lv, "A review of estimation for vehicle tire-road interactions toward automated driving," *IEEE Transactions on Systems, Man, and Cybernetics: Systems*, vol. 49, no. 1, pp. 14–30, 2018.
- [2] T. Kim and S.-K. Ryu, "Review and analysis of pothole detection methods," *Journal of Emerging Trends in Computing and Information Sciences*, vol. 5, no. 8, pp. 603–608, 2014.
- [3] R. Fan, U. Ozgunalp, B. Hosking, M. Liu, and I. Pitas, "Pothole detection based on disparity transformation and road surface modeling," *IEEE Transactions on Image Processing*, vol. 29, pp. 897–908, 2019.
- [4] R. Fan, H. Wang, Y. Wang, M. Liu, and I. Pitas, "Graph attention layer evolves semantic segmentation for road pothole detection: A benchmark and algorithms," *IEEE transactions on image processing*, vol. 30, pp. 8144–8154, 2021.
- [5] A. Wang, H. Lang, Z. Chen, Y. Peng, S. Ding, and J. J. Lu, "The two-step method of pavement pothole and raveling detection and segmentation based on deep learning," *IEEE Transactions on Intelligent Transportation Systems*, 2024.
- [6] L. Li, J. Liu, J. Xing, Z. Liu, K. Lin, and B. Du, "Road pothole detection based on crowdsourced data and extended mask r-cnn," *IEEE Transactions on Intelligent Transportation Systems*, 2024.
- [7] S. Guo, J. Li, Y. Feng, D. Zhou, D. Zhang, C. Chen, S. Su, X. Zhu, Q. Chen, and R. Fan, "Udtiri: An online open-source intelligent road inspection benchmark suite," *IEEE Transactions on Intelligent Transportation Systems*, 2024.
- [8] A. Dosovitskiy, G. Ros, F. Codevilla, A. Lopez, and V. Koltun, "Carla: An open urban driving simulator," in *Conference on robot learning*. PMLR, 2017, pp. 1–16.
- [9] W. Xu and F. Zhang, "Fast-lid: A fast, robust lidar-inertial odometry package by tightly-coupled iterated kalman filter," *IEEE Robotics and Automation Letters*, vol. 6, no. 2, pp. 3317–3324, 2021.
- [10] R. Fan *et al.*, "Road surface 3D reconstruction based on dense subpixel disparity map estimation," *IEEE Transactions on Image Processing*, vol. 27, no. 6, pp. 3025–3035, 2018.
- [11] N. Ma, J. Fan, W. Wang, J. Wu, Y. Jiang, L. Xie, and R. Fan, "Computer vision for road imaging and pothole detection: a state-of-the-art review of systems and algorithms," *Transportation safety and Environment*, vol. 4, no. 4, p. tda026, 2022.
- [12] Y. Hu and T. Furukawa, "Degenerate near-planar 3d reconstruction from two overlapped images for road defects detection," *Sensors*, vol. 20, no. 6, p. 1640, 2020.
- [13] G. Jog, C. Koch, M. Golparvar-Fard, and I. Brilakis, "Pothole properties measurement through visual 2d recognition and 3d reconstruction," in *Computing in Civil Engineering (2012)*, 2012, pp. 553–560.
- [14] M. U. U. Haq, M. Ashfaq, S. Mathavan, K. Kamal, and A. Ahmed, "Stereo-based 3d reconstruction of potholes by a hybrid, dense matching scheme," *IEEE Sensors Journal*, vol. 19, no. 10, pp. 3807–3817, 2019.
- [15] J. Laurent, M. Talbot, and M. Doucet, "Road surface inspection using laser scanners adapted for the high precision 3d measurements of large flat surfaces," in *Proceedings. International conference on recent advances in 3-D digital imaging and modeling (Cat. No. 97TB100134)*. IEEE, 1997, pp. 303–310.
- [16] A. Ahmed, M. Ashfaq, M. U. U. Haq, S. Mathavan, K. Kamal, and M. Rahman, "Pothole 3d reconstruction with a novel imaging system and structure from motion techniques," *IEEE Transactions on Intelligent Transportation Systems*, vol. 23, no. 5, pp. 4685–4694, 2021.
- [17] T. Zhao, P. Guo, J. He, and Y. Wei, "A hierarchical scheme of road unevenness perception with lidar for autonomous driving comfort," *IEEE Transactions on Intelligent Vehicles*, 2023.
- [18] T. Shen, G. Schamp, and M. Haddad, "Stereo vision based road surface preview," in *17th International IEEE Conference on Intelligent Transportation Systems (ITSC)*. IEEE, 2014, pp. 1843–1849.
- [19] R. Fan, U. Ozgunalp, Y. Wang, M. Liu, and I. Pitas, "Rethinking road surface 3-d reconstruction and pothole detection: From perspective transformation to disparity map segmentation," *IEEE Transactions on Cybernetics*, vol. 52, no. 7, pp. 5799–5808, 2021.
- [20] D. Santani, J. Njuguna, T. Bills, A. W. Bryant, R. Bryant, J. Ledgard, and D. Gatica-Perez, "Communisense: Crowdsourcing road hazards in nairobi," in *Proceedings of the 17th International Conference on Human-Computer Interaction with Mobile Devices and Services*, 2015, pp. 445–456.
- [21] A. Dhiman, H.-J. Chien, and R. Klette, "A multi-frame stereo vision-based road profiling technique for distress analysis," in *2018 15th International Symposium on Pervasive Systems, Algorithms and Networks (I-SPAN)*. IEEE, 2018, pp. 7–14.
- [22] R. Labayrade, D. Aubert, and J.-P. Tarel, "Real time obstacle detection in stereovision on non flat road geometry through" v-disparity" representation," in *Intelligent Vehicle Symposium, 2002. IEEE*, vol. 2. IEEE, 2002, pp. 646–651.
- [23] Z. Zhang, "Advanced stereo vision disparity calculation and obstacle analysis for intelligent vehicles," Ph.D. dissertation, University of Bristol, 2013.
- [24] Y. Li, C. Papachristou, and D. Weyer, "Road pothole detection system based on stereo vision," in *NAECON 2018-IEEE national aerospace and electronics conference*. IEEE, 2018, pp. 292–297.
- [25] Y. Du, Z. Zhou, Q. Wu, H. Huang, M. Xu, J. Cao, and G. Hu, "A pothole detection method based on 3d point cloud segmentation," in *Twelfth International Conference on Digital Image Processing (ICDIP 2020)*, vol. 11519. SPIE, 2020, pp. 56–64.
- [26] T. Zhao, L. Yang, Y. Xie, M. Ding, M. Tomizuka, and Y. Wei, "Roadbev: Road surface reconstruction in bird's eye view," *arXiv preprint arXiv:2404.06605*, 2024.
- [27] T. Zhao, C. Xu, M. Ding, M. Tomizuka, W. Zhan, and Y. Wei, "Rsr: A road surface reconstruction dataset and benchmark for safe and comfortable autonomous driving," *arXiv preprint arXiv:2310.02262*, 2023.
- [28] C. Szegedy, V. Vanhoucke, S. Ioffe, J. Shlens, and Z. Wojna, "Rethinking the inception architecture for computer vision," in *Proceedings of the IEEE conference on computer vision and pattern recognition*, 2016, pp. 2818–2826.
- [29] A. G. Howard, "Mobilenets: Efficient convolutional neural networks for mobile vision applications," *arXiv preprint arXiv:1704.04861*, 2017.
- [30] K. He, X. Zhang, S. Ren, and J. Sun, "Deep residual learning for image recognition," in *Proceedings of the IEEE conference on computer vision and pattern recognition*, 2016, pp. 770–778.
- [31] T. Lin, "Focal loss for dense object detection," *arXiv preprint arXiv:1708.02002*, 2017.
- [32] C. Chun and S.-K. Ryu, "Road surface damage detection using fully convolutional neural networks and semi-supervised learning," *Sensors*, vol. 19, no. 24, p. 5501, 2019.
- [33] S. Masihullah, R. Garg, P. Mukherjee, and A. Ray, "Attention based coupled framework for road and pothole segmentation," in *2020 25th International Conference on Pattern Recognition (ICPR)*. IEEE, 2021, pp. 5812–5819.
- [34] Y. Lu, X. Huang, K. Zhang, S. Maharjan, and Y. Zhang, "Communication-efficient federated learning for digital twin edge networks in industrial iot," *IEEE Transactions on Industrial Informatics*, vol. 17, no. 8, pp. 5709–5718, 2020.
- [35] Y. Cheng, Y. Zhang, P. Ji, W. Xu, Z. Zhou, and F. Tao, "Cyber-physical integration for moving digital factories forward towards smart manufacturing: a survey," *The International Journal of Advanced Manufacturing Technology*, vol. 97, pp. 1209–1221, 2018.
- [36] Y. H. Son, G.-Y. Kim, H. C. Kim, C. Jun, and S. D. Noh, "Past, present, and future research of digital twin for smart manufacturing," *Journal of Computational Design and Engineering*, vol. 9, no. 1, pp. 1–23, 2022.
- [37] M. Alazab, L. U. Khan, S. Koppu, S. P. Ramu, M. Iyapparaja, P. Boobalan, T. Baker, P. K. R. Maddikunta, T. R. Gadekallu, and A. Aljuhani, "Digital twins for healthcare 4.0—recent advances, architecture, and open challenges," *IEEE Consumer Electronics Magazine*, vol. 12, no. 6, pp. 29–37, 2022.
- [38] H. Xia, Z. Liu, M. Efremochkina, X. Liu, and C. Lin, "Study on city digital twin technologies for sustainable smart city design: A review and bibliometric analysis of geographic information system and building information modeling integration," *Sustainable Cities and Society*, vol. 84, p. 104009, 2022.
- [39] C. Chen, B. Liu, S. Wan, P. Qiao, and Q. Pei, "An edge traffic flow detection scheme based on deep learning in an intelligent transportation system," *IEEE Transactions on Intelligent Transportation Systems*, vol. 22, no. 3, pp. 1840–1852, 2020.
- [40] Z. Lv, J. Guo, A. K. Singh, and H. Lv, "Digital twins based vr simulation for accident prevention of intelligent vehicle," *IEEE Transactions on Vehicular Technology*, vol. 71, no. 4, pp. 3414–3428, 2022.
- [41] M. D. Jenkins, T. A. Carr, M. I. Iglesias, T. Buggy, and G. Morison, "A deep convolutional neural network for semantic pixel-wise segmentation of road and pavement surface cracks," in *2018 26th European signal processing conference (EUSIPCO)*. IEEE, 2018, pp. 2120–2124.
- [42] X. Wang, Y. Zhang, H. Li, C. Wang, and P. Feng, "Applications and challenges of digital twin intelligent sensing technologies for asphalt pavements," *Automation in Construction*, vol. 164, p. 105480, 2024.
- [43] R. Fan, Y. Zhang, S. Guo, J. Li, Y. Feng, S. Su, Y. Zhang, W. Wang, Y. Jiang, M. J. Bocus *et al.*, "Urban digital twins for intelligent road

- inspection,” in *2022 IEEE International Conference on Big Data (Big Data)*. IEEE, 2022, pp. 5110–5114.
- [44] T. Cao, Y. Wang, and S. Liu, “Pavement crack detection based on 3d edge representation and data communication with digital twins,” *IEEE Transactions on Intelligent Transportation Systems*, vol. 24, no. 7, pp. 7697–7706, 2022.
- [45] C. Sierra, S. Paul, A. Rahman, and A. Kulkarni, “Development of a cognitive digital twin for pavement infrastructure health monitoring,” *Infrastructures*, vol. 7, no. 9, p. 113, 2022.
- [46] W. Wang, X. Xu, J. Peng, W. Hu, and D. Wu, “Fine-grained detection of pavement distress based on integrated data using digital twin,” *Applied Sciences*, vol. 13, no. 7, p. 4549, 2023.
- [47] A. Bono, L. D’Alfonso, G. Fedele, A. Filice, and E. Natalizio, “Path planning and control of a uav fleet in bridge management systems,” *Remote Sensing*, vol. 14, no. 8, p. 1858, 2022.
- [48] R. Mei, W. Sui, J. Zhang, Q. Zhang, T. Peng, and C. Yang, “Rome: Towards large scale road surface reconstruction via mesh representation,” *arXiv preprint arXiv:2306.11368*, 2023.
- [49] W. Wu, Q. Wang, G. Wang, J. Wang, T. Zhao, Y. Liu, D. Gao, Z. Liu, and H. Wang, “Emie-map: Large-scale road surface reconstruction based on explicit mesh and implicit encoding,” *arXiv preprint arXiv:2403.11789*, 2024.
- [50] T. Ren, S. Liu, A. Zeng, J. Lin, K. Li, H. Cao, J. Chen, X. Huang, Y. Chen, F. Yan *et al.*, “Grounded sam: Assembling open-world models for diverse visual tasks,” *arXiv preprint arXiv:2401.14159*, 2024.
- [51] T. Möller and B. Trumbore, “Fast, minimum storage ray/triangle intersection,” in *ACM SIGGRAPH 2005 Courses*, 2005, pp. 7–es.
- [52] L. P. Chew, “Constrained delaunay triangulations,” in *Proceedings of the third annual symposium on Computational geometry*, 1987, pp. 215–222.
- [53] M. Contributors, “MMSegmentation: Openmmlab semantic segmentation toolbox and benchmark,” <https://github.com/open-mmlab/mmssegmentation>, 2020.
- [54] B. Cheng, I. Misra, A. G. Schwing, A. Kirillov, and R. Girdhar, “Masked-attention mask transformer for universal image segmentation,” 2022.
- [55] I. Loshchilov, “Decoupled weight decay regularization,” *arXiv preprint arXiv:1711.05101*, 2017.
- [56] L.-C. Chen, G. Papandreou, I. Kokkinos, K. Murphy, and A. L. Yuille, “Deeplab: Semantic image segmentation with deep convolutional nets, atrous convolution, and fully connected crfs,” *IEEE transactions on pattern analysis and machine intelligence*, vol. 40, no. 4, pp. 834–848, 2017.
- [57] H. Zhao, J. Shi, X. Qi, X. Wang, and J. Jia, “Pyramid scene parsing network,” in *CVPR*, 2017.
- [58] E. Xie, W. Wang, Z. Yu, A. Anandkumar, J. M. Alvarez, and P. Luo, “Segformer: Simple and efficient design for semantic segmentation with transformers,” *arXiv preprint arXiv:2105.15203*, 2021.
- [59] M.-H. Guo, C.-Z. Lu, Q. Hou, Z. Liu, M.-M. Cheng, and S.-M. Hu, “Segnext: Rethinking convolutional attention design for semantic segmentation,” *arXiv preprint arXiv:2209.08575*, 2022.
- [60] X. Chu, Z. Tian, Y. Wang, B. Zhang, H. Ren, X. Wei, H. Xia, and C. Shen, “Twins: Revisiting spatial attention design in vision transformers,” *arXiv preprint arXiv:2104.13840*, 2021.
- [61] T. Xiao, Y. Liu, B. Zhou, Y. Jiang, and J. Sun, “Unified perceptual parsing for scene understanding,” in *Proceedings of the European Conference on Computer Vision (ECCV)*, 2018, pp. 418–434.
- [62] Y. Sun, W. Zuo, and M. Liu, “Rtfnnet: Rgb-thermal fusion network for semantic segmentation of urban scenes,” *IEEE Robotics and Automation Letters*, vol. 4, no. 3, pp. 2576–2583, 2019.
- [63] C. Hazirbas, L. Ma, C. Domokos, and D. Cremers, “Fusenet: Incorporating depth into semantic segmentation via fusion-based cnn architecture,” in *Computer Vision—ACCV 2016: 13th Asian Conference on Computer Vision, Taipei, Taiwan, November 20–24, 2016, Revised Selected Papers, Part I 13*. Springer, 2017, pp. 213–228.
- [64] Q. Ha, K. Watanabe, T. Karasawa, Y. Ushiku, and T. Harada, “Mfnet: Towards real-time semantic segmentation for autonomous vehicles with multi-spectral scenes,” in *2017 IEEE/RSJ International Conference on Intelligent Robots and Systems (IROS)*. IEEE, 2017, pp. 5108–5115.
- [65] R. Fan, H. Wang, P. Cai, and M. Liu, “Sne-roadseg: Incorporating surface normal information into semantic segmentation for accurate freespace detection,” in *European Conference on Computer Vision*. Springer, 2020, pp. 340–356.
- [66] J. Li, Y. Zhan, P. Yun, G. Zhou, Q. Chen, and R. Fan, “Roadformer: Duplex transformer for rgb-normal semantic road scene parsing,” *IEEE Transactions on Intelligent Vehicles*, 2024.
- [67] J.-R. Chang and Y.-S. Chen, “Pyramid stereo matching network,” in *Proceedings of the IEEE conference on computer vision and pattern recognition*, 2018, pp. 5410–5418.
- [68] H. Xu and J. Zhang, “Aanet: Adaptive aggregation network for efficient stereo matching,” in *Proceedings of the IEEE/CVF conference on computer vision and pattern recognition*, 2020, pp. 1959–1968.
- [69] X. Jing, H. Jiang, S. Niu, H. Zhang, B. G. Murengami, Z. Wu, R. Li, C. Zhou, H. Ye, J. Chen *et al.*, “End-to-end stereo matching network with two-stage partition filtering for full-resolution depth estimation and precise localization of kiwifruit for robotic harvesting,” *Computers and Electronics in Agriculture*, vol. 225, p. 109333, 2024.
- [70] G. Xu, X. Wang, X. Ding, and X. Yang, “Iterative geometry encoding volume for stereo matching,” in *Proceedings of the IEEE/CVF Conference on Computer Vision and Pattern Recognition*, 2023, pp. 21919–21928.
- [71] C.-W. Liu, Q. Chen, and R. Fan, “Playing to vision foundation model’s strengths in stereo matching,” *arXiv preprint arXiv:2404.06261*, 2024.
- [72] A. Geiger, P. Lenz, C. Stiller, and R. Urtasun, “Vision meets robotics: The kitti dataset,” *The International Journal of Robotics Research*, vol. 32, no. 11, pp. 1231–1237, 2013.
- [73] W. Zeng and R. L. Church, “Finding shortest paths on real road networks: the case for a,” *International journal of geographical information science*, vol. 23, no. 4, pp. 531–543, 2009.
- [74] S. Karaman and E. Frazzoli, “Incremental sampling-based algorithms for optimal motion planning,” 2011.
- [75] T. M. Howard, C. J. Green, A. Kelly, and D. Ferguson, “State space sampling of feasible motions for high-performance mobile robot navigation in complex environments,” *Journal of Field Robotics*, vol. 25, no. 6-7, pp. 325–345, 2008.
- [76] D. Dolgov, S. Thrun, M. Montemerlo, and J. Diebel, “Practical search techniques in path planning for autonomous driving,” *Ann Arbor*, vol. 1001, no. 48105, pp. 18–80, 2008.
- [77] B. Kerbl, G. Kopanas, T. Leimkühler, and G. Drettakis, “3d gaussian splatting for real-time radiance field rendering,” 2023. [Online]. Available: <https://arxiv.org/abs/2308.04079>



Yikang Zhang received the B.Sc. degree in Automation from the Beijing Institute of Technology in 2017, and the M.S. degree in Electronics and Computer Engineering, UMASS Amherst in 2019. He is currently pursuing the Ph.D degree in Shanghai Research Institute for Intelligent Autonomous Systems, Tongji University, supervised by Prof. Rui Fan. His current research mainly focuses on 3D reconstruction for autonomous driving.



Chuang-Wei Liu received his B.E. degree in automation from Tongji University in 2020. He is currently pursuing his Ph.D. degree, supervised by Prof. Rui Fan, with the Machine Intelligence and Autonomous Systems (MIAS) Group in the Robotics and Artificial Intelligence Laboratory (RAIL) at Tongji University. His research interests include computer stereo vision, especially for unsupervised approaches, and long-term learning. He is currently a student member of IEEE.



Jiahang Li (Graduate Student Member, IEEE) received his B.Eng. degree in automation from Taiyuan University of Technology in 2021. He is currently pursuing his Master's degree, under the supervision of Prof. Rui Fan, with the Machine Intelligence and Autonomous Systems (MIAS) Group in the Robotics and Artificial Intelligence Laboratory (RAIL) at Tongji University. His research interests include computer vision and deep learning.



Yingbing Chen received the B.Sc. degree from Northwestern Polytechnical University, Xian, China, in 2015, and the the M.S. degree from Xiamen University, Xiamen, China, in 2018. He received his Ph.D. degree from Hong Kong University of Science and Technology in 2024. His current research interests include machine learning, motion and behavioral planning for autonomous driving and robotics.



Jie Cheng received the B.S. degree from Huazhong University of Science and Technology, Wuhan, China, in 2019. He received the Ph.D. degree in 2024 from the Hong Kong University of Science and Technology, HKSAR, China, supervised by Prof. Qifeng Chen. His research mainly focuses on motion planning and motion forecasting for autonomous driving.



Rui Fan (Senior Member, IEEE) received the B.Eng. degree in Automation from the Harbin Institute of Technology in 2015 and the Ph.D. degree in Electrical and Electronic Engineering from the University of Bristol in 2018. He worked as a Research Associate at the Hong Kong University of Science and Technology from 2018 to 2020 and a Postdoctoral Scholar-Employee at the University of California San Diego between 2020 and 2021. He began his faculty career as a Full Research Professor with the College of Electronics & Information Engineering

at Tongji University in 2021, and was then promoted to a Full Professor in the same college, as well as at the Shanghai Research Institute for Intelligent Autonomous Systems in 2022.

Prof. Fan served as an associate editor for ICRA'23/25 and IROS'23/24, an area chair for ICIP'24, and a senior program committee member for AAAI'23/24/25. He is the general chair of the AVVision community and organized several impactful workshops and special sessions in conjunction with WACV'21, ICIP'21/22/23, ICCV'21, and ECCV'22. He was honored by being included in the Stanford University List of Top 2% Scientists Worldwide between 2022 and 2024, recognized on the Forbes China List of 100 Outstanding Overseas Returnees in 2023, and acknowledged as one of Xiaomi Young Talents in 2023. His research interests include computer vision, deep learning, and robotics, with a specific focus on humanoid visual perception under the two-streams hypothesis.